Doping dependence of the magnetic excitations in La$_{2-x}$Sr$_x$CuO$_4$

D. Meyers,[1,*] H. Miao,[1] A. C. Walters,[2] V. Bisogni,[3] R. S. Springell,[4] M. d'Astuto,[5] M. Dantz,[6] J. Pelliciari,[6] H. Y. Huang,[7]
J. Okamoto,[7] D. J. Huang,[7,8] J. P. Hill,[3] X. He,[1,9] I. Božović,[1,9] T. Schmitt,[6] and M. P. M. Dean[1,†]

[1]*Department of Condensed Matter Physics and Materials Science, Brookhaven National Laboratory, Upton, New York 11973, USA*

[2]*Diamond Light Source, Ltd., Harwell Science and Innovation Campus, Chilton, Didcot, Oxfordshire, OX11 0DE, United Kingdom*

[3]*National Synchrotron Light Source II, Brookhaven National Laboratory, Upton, New York 11973, USA*

[4]*Interface Analysis Centre, School of Physics, University of Bristol, Bristol, BS2 8BS, United Kingdom*

[5]*Institut de Minéralogie et de Physique des Milieux Condensés (IMPMC), UMR CNRS 7590, Université Pierre et Marie Curie – Case 115,
4 Place Jussieu, 75252 Paris Cedex 05, France*

[6]*Research Department Synchrotron Radiation and Nanotechnology, Paul Scherrer Institut, CH-5232 Villigen PSI, Switzerland*

[7]*National Synchrotron Radiation Research Center, Hsinchu 30076, Taiwan*

[8]*Department of Physics, National Tsing Hua University, Hsinchu 30013, Taiwan*

[9]*Yale University, Department of Applied Physics, New Haven, Connecticut 06520, USA*

(Received 25 November 2016; revised manuscript received 19 January 2017; published 21 February 2017)

The magnetic correlations within the cuprates have undergone intense scrutiny as part of efforts to understand high-temperature superconductivity. We explore the evolution of the magnetic correlations along the nodal direction of the Brillouin zone in La$_{2-x}$Sr$_x$CuO$_4$, spanning the doping phase diagram from the antiferromagnetic Mott insulator at $x = 0$ to the metallic phase at $x = 0.26$. Magnetic excitations along this direction are found to be systematically softened and broadened with doping, at a higher rate than the excitations along the antinodal direction. This phenomenology is discussed in terms of the nature of the magnetism in the doped cuprates. Survival of the high-energy magnetic excitations, even in the overdoped regime, indicates that these excitations are marginal to pairing, while the influence of the low-energy excitations remains ambiguous.

I. INTRODUCTION

The past several decades have witnessed a considerable scientific effort within the condensed matter community to unravel the true origin of high-temperature superconductivity (HTS) [1–4]. Due to the proximity of antiferromagnetic order and HTS in the doping phase diagram, as shown in Fig. 1(a), the relationship between magnetism and superconductivity has been discussed extensively. This even includes postulating that superconducting pairing is driven by the exchange of magnetic excitations, although putting such a scenario on firm theoretical footing remains very challenging [5]. What is clear, however, is that the Coulomb repulsion U plays a dominant role in the formation of the antiferromagnetic (AFM) insulating state in the cuprate parent compounds and that this leads to the emergence of a well-defined spin wave or magnon excitations [6–14]. These disperse up to very high energies (about 300 meV) along the antinodal direction in the Brillouin zone [$(0,0) \rightarrow (0.5,0)$ in commonly used tetragonal notation] and up to comparable but somewhat lower energies along the nodal [$(0,0) \rightarrow (0.25,0.25)$] direction. Such a large energy scale would naturally be expected to play a central role over a large fraction of the phase diagram. There have consequently been extensive efforts to characterize the nature of magnetism across the cuprate phase diagram [11,12,15–29], which have demonstrated that substantial magnetic spectral weight persists to at least optimal doping (i.e., a hole concentration $x \approx 0.15$). A more controversial issue is what happens for the overdoped cuprates with hole concentration $0.15 \lesssim x \lesssim 0.3$. In this

doping range inelastic neutron scattering (INS) indicates that the energy ω and wave vector $\boldsymbol{Q}$ integrated magnetic spectral weight is strongly reduced [30]. This even encompasses discussions of whether magnetism might effectively disappear completely in the overdoped regime and whether this might be the reason that HTS is suppressed at a similar doping level [3,31,32]. More extensive studies of the overdoped cuprates, and how their excitations relate to the magnons in the parent compounds, are therefore desirable. In recent years resonant inelastic x-ray scattering (RIXS) [12,33] has emerged as a complementary tool to INS in the investigation of magnetic excitations in the cuprates [11,12,21,23–26,28,29]. In particular, RIXS offers the possibility to probe very small sample volumes [10] and to perform more extensive doping dependence, as the large single-crystal samples required for INS are often highly challenging to produce for overdoped cuprates.

In this article, we use RIXS to investigate La$_{2-x}$Sr$_x$CuO$_4$ (LSCO) along the nodal direction of the Brillouin zone in samples spanning the AFM insulating to overdoped superconducting phases in order to unravel the doping systematics of the magnetic excitations. Combined with our previous equivalent data along the antinodal direction [10,11], this constitutes an extensive characterization of the high-energy magnetic excitation spectrum throughout the LSCO phase diagram. In this article we will refer to damped magnetic excitations that evolve from the magnon excitation in the insulator as paramagnons. Our use of this term is not meant to imply anything about the presence or absence of magnetic order. We find a gradual softening and broadening of the paramagnon feature with doping. The high-energy magnetic excitations studied here do not show any strong changes that correlate with the suppression of superconductivity in the
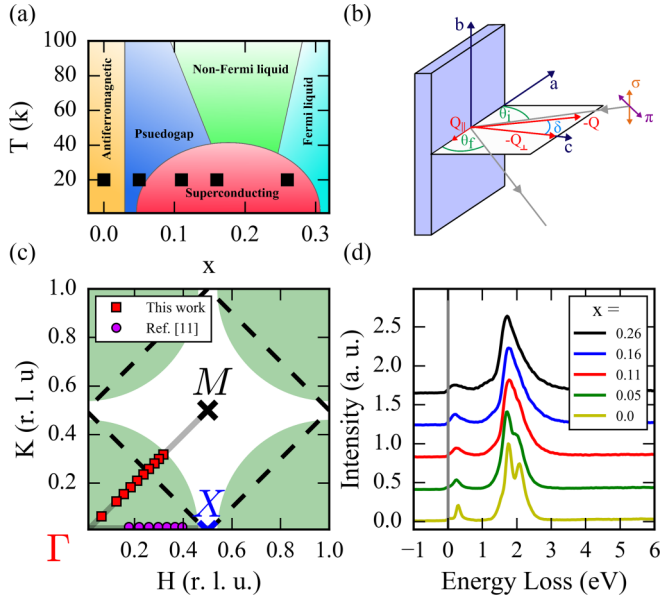
*dmeyers@bnl.gov
†mdean@bnl.gov

FIG. 1. (a) Doping phase diagram for LSCO. (b) RIXS geometry used for the experiment. (c) Plot of the cuprate Brillouin zone. Red squares represent $\boldsymbol{Q}$ points measured for this report, and purple circles for previous work by this group [11]. The green semicircles represent the regions of reciprocal space accessible to Cu L_3-edge RIXS. (d) RIXS spectra for each doping at $\boldsymbol{Q} = (0.24, 0.24)$ showing dd excitation and paramagnon features. Data are offset vertically for clarity. The gray line denotes the zero-energy-loss position.

overdoped regime, consistent with previous work asserting that these modes have a marginal role in HTS [11]. This is notably different from the low-energy AFM correlations around (0.5,0.5) which *are* strongly modified in the overdoped regime. Qualitatively similar differences between the nodal and antinodal directions are captured by calculations of the magnetic excitation spectrum based on itinerant quasiparticles, which is discussed in terms of conceptualizing magnetism in the overdoped cuprates [23,34–37].

II. EXPERIMENTAL METHODS

Thin-film LSCO samples were synthesized on single-crystal LaSrAlO$_4$ substrates with atomic layer-by-layer molecular beam epitaxy [38]. Typical surface root-mean-square roughnesses, as determined by atomic force microscopy, were about 3 Å, which helps to reduce the contribution of diffuse elastic scattering to the RIXS spectra. The sample thicknesses for $x = 0$, 0.05, 0.11, 0.16, and 0.26 were 53, 79, 99, 53, and 99 nm, respectively, as determined by measuring the Kiessig fringes in x-ray diffraction, consistent with counting the layers during the growth process. The RIXS data presented were collected using the SAXES spectrometer [39] at the ADRESS beamline [40] of the Swiss Light Source at the Paul Scherrer Institute. Further checks were performed at the AGS-AGM spectrometer [41] at BL05A1 – the Inelastic Scattering beamline at the National Synchrotron Radiation Research Center, Taiwan. Energy resolution measurements carried out on carbon tape immediately before sample measurements gave an overall energy resolution of ∼120 meV FWHM and served as a

reference for the zero energy loss calibration. All data shown were collected at low temperature (approximately 20 K).

Figure 1(b) displays the horizontal scattering geometry used for this study. The momentum transferred in-plane was varied by changing the incident angle θ_i, giving $\boldsymbol{Q}_\parallel = 2|\boldsymbol{k}_i|\sin(2\theta/2)\sin(\delta)$, where $\delta = 2\theta/2 - \theta_i$. The x-ray scattering angle 2θ was fixed at 130° and measurements were taken with grazing exit geometry ($\theta_i > 65°$) and horizontal incident x-ray polarization equivalent to previous studies [11,21,23,24,42]. Figure 1(c) plots the two-dimensional Brillouin zone as a function of $\boldsymbol{Q} = (H, K)$, which is defined in terms of the high-temperature tetragonal unit cell with $a = b \approx 3.8$ Å. Within this study, measurements were taken along the nodal direction (from Γ towards M), which we consider in the context of previously collected data taken along the antinodal direction (from Γ towards X) [11].

III. RESULTS AND ANALYSIS

Figure 1(d) shows example RIXS spectra at $\boldsymbol{Q} = (0.24, 0.24)$ as a function of doping. La$_2$CuO$_4$ shows a small elastic feature with sharp magnetic and well-defined dd features consistent with the localized insulating nature of the parent compound. As the doping traverses the antiferromagnetic (AFM), pseudogap and spin-glass ($x = 0.05$), and under- and overdoped superconducting regions the dd features become broadened [30].

Magnetic excitations along the nodal direction in the Brillouin zone in the parent compound La$_2$CuO$_4$ have been studied in detail and can be adequately modeled using spin-wave theory [6,7,9,10]. In RIXS spectra these spin-wave or magnon excitations are present alongside an optical phonon and high-energy magnetic continuum [7,8,10,12]. We performed a similar analysis to that used previously in Refs. [11,12,21,24,42] in order to facilitate direct comparisons with previous work. An example fit is shown in Fig. 2(a). Here, the magnon and magnetic continuum features were modeled with an antisymmetrized Lorentzian convolved with a Gaussian resolution function with FWHM ∼120 meV [Fig. 2(a)].[1] The antisymmetrized Lorentzian is used to account for the time reversal symmetry of the imaginary part of the dynamical susceptibility, $\chi''(\boldsymbol{Q}, \omega)$. Following previous work, this is proportional to the scattering function corrected by the Bose factor,

$$S(\boldsymbol{Q}, \omega) \propto \frac{\chi''(\boldsymbol{Q}, \omega)}{1 - \exp(-\omega/k_B T)}, \qquad (1)$$

where $k_B T$ is the thermal energy scale [11,21,24]. The elastic scattering and optical phonon were fit with Gaussian functions. Finally, a smooth background was fit with a third-order polynomial to account for the tail of the dd excitations that carry much higher intensity [see Fig. 1(d)]. This model provides a good description of the spectral line shape for the $x = 0$ insulator below 1 eV. The broader features at higher dopings makes it impossible to convincingly separate the multimagnon and the phonon features from the paramagnon,

---

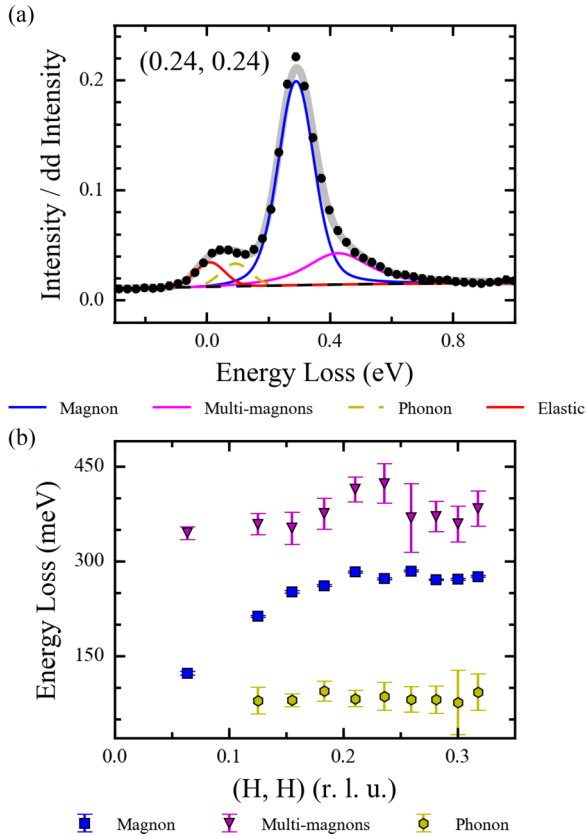[1]See the Supplemental Material of Ref. [11] for a explicit definition of the function.

FIG. 2. La$_2$CuO$_4$ RIXS spectra. (a) An example spectrum at $Q =$ (0.24,0.24) showing the different components of the fit including magnon, multimagnon, phonon, and elastic as well as the total fit in gray. (b) Dispersion of the phonon, multimagnon, and single-magnon features.

and we perform fits in which a single peak accounts for all these features to allow for direct comparison with previous work [11,21,24]. We also note that a recent report discussed the appropriateness of this widely used scheme in the case of heavily overdamped modes [43]. We examined this issue in detail as described in the Supplemental Material, concluding that the functional form we use is adequate for the damping rates found in this study [44].

Figure 2(b) shows the fitting results for La$_2$CuO$_4$ ($x = 0$). A dispersive magnon is observed with a maximum energy transfer of ∼290 meV around the Brillouin zone boundary, consistent with spin-wave theory predictions based on INS [6,9] and previous RIXS studies [10]. The magnetic continuum feature is challenging to unambiguously separate from the magnon, but, as expected, it lies at higher energies and is less dispersive than the magnon. The 90-meV feature has negligible Q dependence (≲25 meV), limited by the error bars, consistent with it being an optical phonon [45–47].

We now discuss the doping evolution of the nodal excitations, plotted as a color map in Fig. 3. Low-energy spectral features are visible for all studied dopings. Detailed incident energy dependence has confirmed the magnetic nature of these spectral features [28,48], consistent with theoretical calculations [49] and the smooth evolution of these features with respect to the unambiguously magnetic feature in La$_2$CuO$_4$.
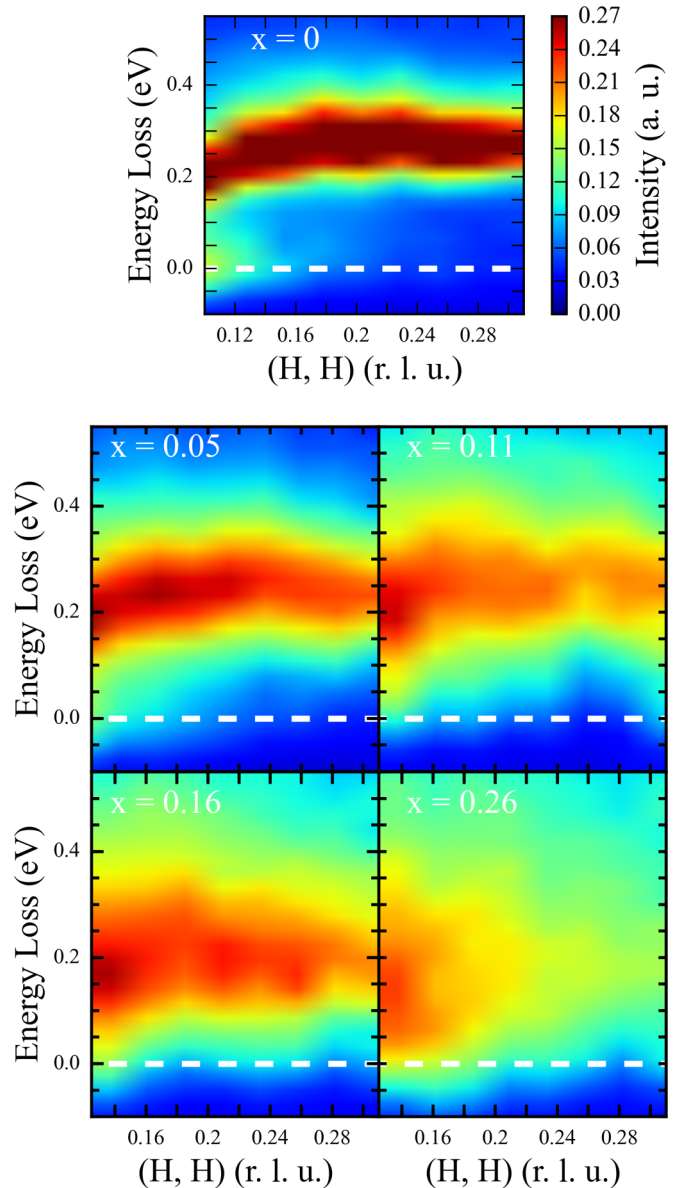

FIG. 3. Plots of the RIXS spectra dispersion for each doping represented as a two-dimensional color map. The broadening of the paramagnon feature with increased doping is readily apparent. All panels share the same intensity scale as shown on the top panel. The doping x is noted in white in the top-left corner of every panel.

Future experiments that explicitly resolve the scattered x-ray polarization would be a valuable addition to this issue [50]. In comparison to the parent compound, the magnetic spectral weight is broadened and appears to be softened. Both these effects appear to occur continuously as the doping spans the phase diagram from the pseudogap ($x = 0.05$), underdoped ($x = 0.11$), nearly optimal ($x = 0.16$), and all the way to the overdoped phase ($x = 0.26$). This phenomenology is consistent with previous examinations of the nodal dispersion in Bi$_2$Sr$_2$Ca$_{n-1}$Cu$_n$O$_{2n+4+\delta}$ [24,25,28] and LSCO ($x = 0.26$, 0.30) [26,29]. The present data, alongside Ref. [11], provide the first comprehensive RIXS study of undoped, underdoped, optimally doped, and overdoped samples within a single cuprate system. The characteristic energy of the excitations
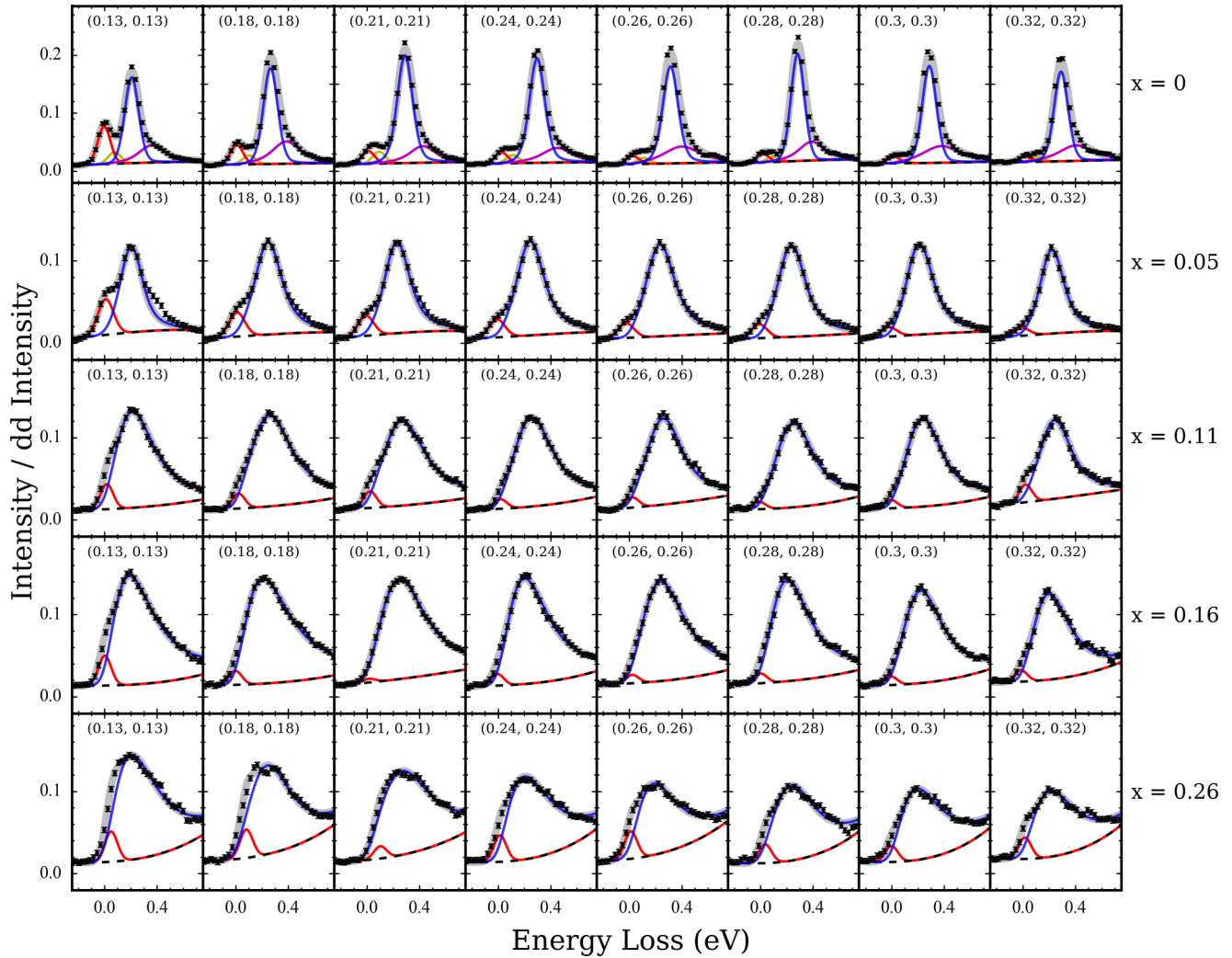
FIG. 4. Individual RIXS spectra for each sample (horizontal) and every Q point (vertical) with underlain fit. For all samples except the parent compound only the elastic (red), paramagnon (blue), and smooth background (dashed black) were used as components in the fit. The features of the spectra are displayed added to the background from the dd excitations. The total fit is represented by a gray line. For the $x = 0$ case, the multimagnon feature is shown in purple, which was not resolved for the doped samples. The detailed fitting procedure is discussed in the text.

was addressed in more detail by fitting analysis as shown in Fig. 4. As can be seen, the fitting procedure is able to reliably reproduce the experimental curves, despite the significant broadening at higher dopings.

Figure 5 provides the values from the least-squares fitting analysis. A softening of the paramagnon mode with doping in Fig. 5(a) is very apparent, with the overdoped sample in particular showing a significant drop of around 80 ± 10 meV, with respect to $x = 0$, at high Q. The paramagnon energy also becomes progressively less Q dependent with doping. We extracted a characteristic energy scale for the excitations by fitting a sinusoidal function [6], Fig. 6, to the Q dependence at different x and plot the results in Fig. 5(d).[2] The maximum energy transfer follows a nearly linear dependence upon doping, irrespective of the notable changes in the electronic state

of the sample (i.e., insulating, pseudogap, superconducting). Moving to the paramagnon width [Fig. 5(b)], fitting the $x = 0$ spectrum yields a value of around 75 meV, which is likely to come from difficulties separating contributions from phonons and the magnetic continuum from the magnetic pole [11] and should be thought of as an upper limit on the width. Upon doping the average width [Fig. 5(e)] increases strongly. The integrated spectral intensity, normalized to the dd intensity [Fig. 5(c)], peaks at intermediate Q values and persists without strong changes as a function of doping.[3] Self-absorption can satisfactorily explain the decrease towards higher Q, as the x-ray emission angle is progressively lowered. Figures 5(e) and 5(f) show that the spectra broaden continuously with

---

[2]The undoped dispersion function with fixed magnetic exchange and a variable maximum energy transfer was used for the fitting.

[3]For the $x = 0$ case, the phonon and multimagnon intensities were included with the paramagnon intensity, as these were not distinguishable for the higher dopings.
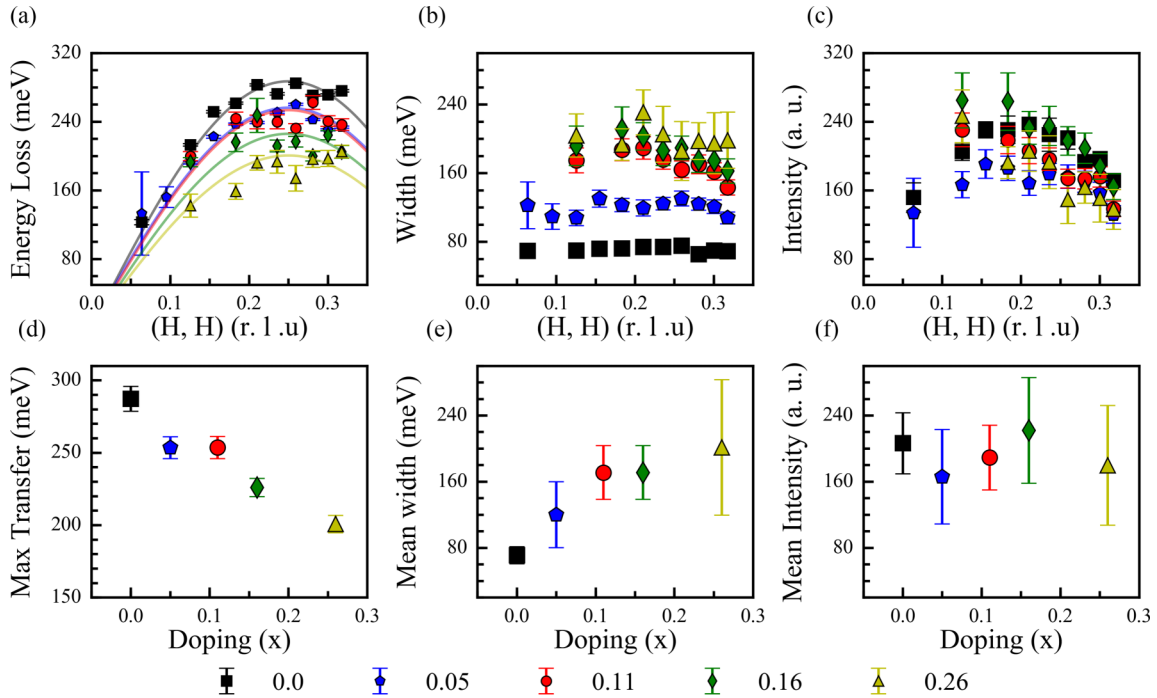
FIG. 5. (a) The paramagnon dispersion for each doping with applied fit. (b) Paramagnon peak width for each Q point defined as a Lorentzian half-width at half-maximum (HWHM). (c) Paramagnon spectral weight for each sample and Q point. (d) Maximum energy transfer for each doping. (e) Q-averaged widths with cumulative error. (f) Q-averaged intensities. The error bars represent the statistical error from the fitting procedure.

increasing doping without strong changes in integrated spectral weight.

IV. DISCUSSION

A comparison between the nodal and antinodal dispersions, and how they relate to the dispersion in the parent compound,
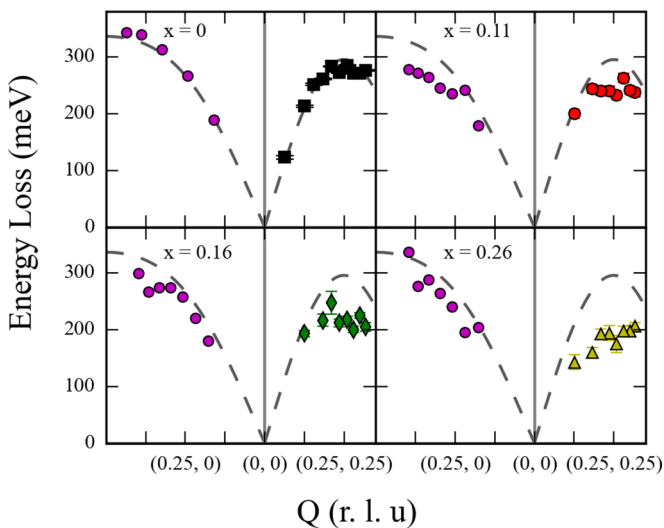

FIG. 6. Comparison of the nodal and antinodal [10,11] data for each doping. Dashed lines represent the spin-wave theory predictions for La$_2$CuO$_4$. $x = 0.05$ was not previously measured.

is presented in Fig. 6. The dashed line represents the dispersion from spin-wave theory for La$_2$CuO$_4$ [6]. Both the nodal and antinodal directions are shown, with the results for the same samples from a previous work displayed as purple circles [10,11]. Dispersive magnetic excitations are clearly present for all dopings, albeit with strongly reduced dispersion, particularly in the nodal direction. This extends the discussion of the behavior of the magnetic excitations in the antinodal direction [11] to the nodal direction within the Brillouin zone. It is clear that the overdoped cuprates do not become trivial, completely nonmagnetic, Fermi liquids. Rather, the effects of U still appear to be present in the form of strongly damped high-energy magnetic excitations within the region in reciprocal space we have studied [shown in Fig. 1(c)].

These results help constrain theoretical models of magnetism in the cuprates. The Hubbard model, in either its one- or three-band variants, is often considered to be the best-justified starting point for modeling magnetism in the cuprates (and strongly correlated materials more generally) [2]. Calculations of the Hubbard model indeed capture the persistent high-energy magnetic excitations in good accord with experiments [49,51]. However, such calculations are typically confined to small lattices and there is significant interest in conceptualizing magnetism in terms of either local moment [52,53] or (renormalized) itinerant quasiparticle methods [23,34–37]. A local-moment-based approach is well justified in La$_2$CuO$_4$ and has been used a lot in terms of describing stripe physics in the underdoped regime [52]. Such an approach also naturally explains why the intensity

of the excitations in the doped cuprates is of a comparable magnitude to those in the insulator. Itinerant quasiparticle pictures, in which correlations are treated within several different approximate schemes, are also popular. These have a significant advantage in terms of allowing predictions with high Q resolution [23,29,34–37]. They also capture the fact that the nodal excitations are more strongly doping dependent than the antinodal excitations, as observed here.

It is also important to consider the data presented here in the context of previous INS measurements [6,9,12,15–20,26]. Spin-wave theory for AFM La_2CuO_4 implies that the dispersion around (0,0) and (0.5,0.5) should be symmetric. On this basis, it is tempting to compare RIXS and INS data on doped cuprates assuming this symmetry. Figure 6 shows that for $x = 0.26$ the magnetic excitations at wave vectors accessed by RIXS around (0,0) have a significantly lower energy scale than excitations seen by neutrons around (0.5,0.5) [26], suggesting that this symmetry breaks down in the doped cuprates and such a comparison appears invalid. Unfortunately, there is very little directly comparable RIXS and INS data taken at the same Q; however, the one available study suggests that both methods provide similar access to magnetic dispersions on the samples with $x = 0.25$ and 0.30 [26]. Our results are consistent with these measurements over a large doping range [11,19,20].

In the context of HTS, we note that the high-energy excitations studied here show minimal changes in going from the optimally doped to the overdoped regime. As such, they further support previous assertions that the high-energy magnetic excitations observed here are marginal to superconducting pairing [11]. This hypothesis tallies with a simple consideration of how a repulsive interaction might contribute to d-wave pairing in the cuprates via transitions between different states near the Fermi level. In such a scenario the excitations around (0.5,0.5) would be expected to have a stronger contribution than excitations elsewhere in Q, and excitations far from (0.5,0.5) can even lead to pair breaking and reduction of T_c [3].

V. CONCLUSIONS

The paramagnon dispersion along the nodal direction in the Brillouin zone is reported for samples spanning the LSCO phase diagram from the AFM insulator to the overdoped superconductor. We found a gradual softening and damping of the paramagnon excitation with doping as predicted by Hubbard model calculations [49,51]. The character of the excitations indicates that magnetic correlations in the cuprates have both localized and itinerant character. These findings further support suggestions that the high-energy magnetic excitations studied here have a marginal role for HTS [11]. Likely, the destruction of other pairing interactions, such as the low-energy magnetic excitations, is instead culpable for the drop in T_c with overdoping.

[1] E. Dagotto, Rev. Mod. Phys. **66**, 763 (1994).

[2] P. A. Lee, N. Nagaosa, and X.-G. Wen, Rev. Mod. Phys. **78**, 17 (2006).

[3] D. J. Scalapino, Rev. Mod. Phys. **84**, 1383 (2012).

[4] B. Keimer, S. Kivelson, M. Norman, S. Uchida, and J. Zaanen, Nature (London) **518**, 179 (2015).

[5] M. Eschrig, Adv. Phys. **55**, 47 (2006).

[6] R. Coldea, S. M. Hayden, G. Aeppli, T. G. Perring, C. D. Frost, T. E. Mason, S.-W. Cheong, and Z. Fisk, Phys. Rev. Lett. **86**, 5377 (2001).

[7] L. Braicovich, J. van den Brink, V. Bisogni, M. M. Sala, L. J. P. Ament, N. B. Brookes, G. M. De Luca, M. Salluzzo, T. Schmitt, V. N. Strocov, and G. Ghiringhelli, Phys. Rev. Lett. **104**, 077002 (2010).

[8] M. Guarise, B. Dalla Piazza, M. Moretti Sala, G. Ghiringhelli, L. Braicovich, H. Berger, J. N. Hancock, D. van der Marel, T. Schmitt, V. N. Strocov, L. J. P. Ament, J. van den Brink, P.-H.

Lin, P. Xu, H. M. Rønnow, and M. Grioni, Phys. Rev. Lett. **105**, 157006 (2010).

[9] N. S. Headings, S. M. Hayden, R. Coldea, and T. G. Perring, Phys. Rev. Lett. **105**, 247001 (2010).

[10] M. P. M. Dean, R. S. Springell, C. Monney, K. J. Zhou, J. Pereiro, I. Božović, B. Dalla Piazza, H. M. Rønnow, E. Morenzoni, J. van den Brink, T. Schmitt, and J. P. Hill, Nat. Mater. **11**, 850 (2012).

[11] M. P. M. Dean, G. Dellea, R. S. Springell, F. Yakhou-Harris, K. Kummer, N. B. Brookes, X. Liu, Y.-J. Sun, J. Strle, T. Schmitt, L. Braicovich, G. Ghiringhelli, I. Bozovic, and J. P. Hill, Nat. Mater. **12**, 1019 (2013).

[12] M. P. M. Dean, J. Magn. Magn. Mater. **376**, 3 (2015).

[13] B. W. Lebert, M. P. M. Dean, A. Nicolaou, J. Pelliciari, M. Dantz, T. Schmitt, R. Yu, M. Azuma, J. Castellan, H. Miao, A. Gauzzi, B. Baptiste, and M. d'Astuto, arXiv:1610.08383.

[14] M. Dantz, J. Pelliciari, D. Samal, V. Bisogni, Y. Huang, P.

Olalde-Velasco, V. Strocov, G. Koster, and T. Schmitt, Sci. Rep. **6**, 32896 (2016).

[15] P. Bourges, Y. Sidis, H. F. Fong, L. P. Regnault, J. Bossy, A. Ivanov, and B. Keimer, Science **288**, 1234 (2000).

[16] J. M. Tranquada, H. Woo, T. G. Perring, H. Goka, G. D. Gu, G. Xu, M. Fujita, and K. Yamada, Nature (London) **429**, 534 (2004).

[17] S. M. Hayden, H. A. Mook, P. Dai, T. G. Perring, and F. Dogan, Nature (London) **429**, 531 (2004).

[18] H. Woo, P. Dai, S. M. Hayden, H. A. Mook, T. Dahm, D. J. Scalapino, T. G. Perring, and F. Dogan, Nat. Phys. **2**, 600 (2006).

[19] O. J. Lipscombe, S. M. Hayden, B. Vignolle, D. F. McMorrow, and T. G. Perring, Phys. Rev. Lett. **99**, 067002 (2007).

[20] B. Vignolle, S. M. Hayden, D. F. McMorrow, H. M. Ronnow, B. Lake, C. D. Frost, and T. G. Perring, Nat. Phys. **3**, 163 (2007).

[21] M. Le Tacon, G. Ghiringhelli, J. Chaloupka, M. M. Sala, V. Hinkov, M. W. Haverkort, M. Minola, M. Bakr, K. J. Zhou, S. Blanco-Canosa, C. Monney, Y. T. Song, G. L. Sun, C. T. Lin, G. M. De Luca, M. Salluzzo, G. Khaliullin, T. Schmitt, L. Braicovich, and B. Keimer, Nat. Phys. **7**, 725 (2011).

[22] V. Bisogni, M. Moretti Sala, A. Bendounan, N. B. Brookes, G. Ghiringhelli, and L. Braicovich, Phys. Rev. B **85**, 214528 (2012).

[23] M. P. M. Dean, A. J. A. James, R. S. Springell, X. Liu, C. Monney, K. J. Zhou, R. M. Konik, J. S. Wen, Z. J. Xu, G. D. Gu, V. N. Strocov, T. Schmitt, and J. P. Hill, Phys. Rev. Lett. **110**, 147001 (2013).

[24] M. P. M. Dean, A. J. A. James, A. C. Walters, V. Bisogni, I. Jarrige, M. Hücker, E. Giannini, M. Fujita, J. Pelliciari, Y. B. Huang, R. M. Konik, T. Schmitt, and J. P. Hill, Phys. Rev. B **90**, 220506 (2014).

[25] M. Guarise, B. Dalla Piazza, H. Berger, E. Giannini, T. Schmitt, H. M. Rønnow, G. Sawatzky, J. Van Den Brink, D. Altenfeld, I. Eremin *et al.*, Nat. Commun. **5**, 5760 (2014).

[26] S. Wakimoto, K. Ishii, H. Kimura, M. Fujita, G. Dellea, K. Kummer, L. Braicovich, G. Ghiringhelli, L. M. Debeer-Schmitt, and G. E. Granroth, Phys. Rev. B **91**, 184513 (2015).

[27] D. S. Ellis, Y.-B. Huang, P. Olalde-Velasco, M. Dantz, J. Pelliciari, G. Drachuck, R. Ofer, G. Bazalitsky, J. Berger, T. Schmitt, and A. Keren, Phys. Rev. B **92**, 104507 (2015).

[28] H. Huang, C. Jia, Z. Chen, K. Wohlfeld, B. Moritz, T. Devereaux, W. Wu, J. Okamoto, W. Lee, M. Hashimoto *et al.*, Sci. Rep. **6**, 19657 (2016).

[29] C. Monney, T. Schmitt, C. E. Matt, J. Mesot, V. N. Strocov, O. J. Lipscombe, S. M. Hayden, and J. Chang, Phys. Rev. B **93**, 075103 (2016).

[30] M. Fujita, H. Hiraka, M. Matsuda, M. Matsuura, J. M. Tranquada, S. Wakimoto, G. Xu, and K. Yamada, J. Phys. Soc. Jpn. **81**, 011007 (2012).

[31] S. Wakimoto, H. Zhang, K. Yamada, I. Swainson, H. Kim, and R. J. Birgeneau, Phys. Rev. Lett. **92**, 217004 (2004).

[32] S. Fujiyama, H. Ohsumi, T. Komesu, J. Matsuno, B. J. Kim, M. Takata, T. Arima, and H. Takagi, Phys. Rev. Lett. **108**, 247212 (2012).

[33] L. J. P. Ament, M. van Veenendaal, T. P. Devereaux, J. P. Hill, and J. van den Brink, Rev. Mod. Phys. **83**, 705 (2011).

[34] A. J. A. James, R. M. Konik, and T. M. Rice, Phys. Rev. B **86**, 100508 (2012).

[35] R. Zeyher and A. Greco, Phys. Rev. B **87**, 224511 (2013).

[36] M. V. Eremin, I. M. Shigapov, and H. T. D. Thuy, J. Phys.: Condens. Matter **25**, 345701 (2013).

[37] W.-J. Li, C.-J. Lin, and T.-K. Lee, Phys. Rev. B **94**, 075127 (2016).

[38] I. Božović, IEEE Trans. Appl. Supercond. **11**, 2686 (2001).

[39] G. Ghiringhelli, A. Piazzalunga, C. Dallera, G. Trezzi, L. Braicovich, T. Schmitt, V. N. Strocov, R. Betemps, L. Patthey, X. Wang, and M. Grioni, Rev. Sci. Instrum. **77**, 113108 (2006).

[40] V. N. Strocov, T. Schmitt, U. Flechsig, T. Schmidt, A. Imhof, Q. Chen, J. Raabe, R. Betemps, D. Zimoch, J. Krempasky, X. Wang, M. Grioni, A. Piazzalunga, and L. Patthey, J. Synchrotron Radiat. **17**, 631 (2010).

[41] C. H. Lai, H. S. Fung, W. B. Wu, H. Y. Huang, H. W. Fu, S. W. Lin, S. W. Huang, C. C. Chiu, D. J. Wang, L. J. Huang, T. C. Tseng, S. C. Chung, C. T. Chen, and D. J. Huang, J. Synchrotron Radiat. **21**, 325 (2014).

[42] M. P. M. Dean, G. Dellea, M. Minola, S. B. Wilkins, R. M. Konik, G. D. Gu, M. Le Tacon, N. B. Brookes, F. Yakhou-Harris, K. Kummer, J. P. Hill, L. Braicovich, and G. Ghiringhelli, Phys. Rev. B **88**, 020403 (2013).

[43] J. Lamsal and W. Montfrooij, Phys. Rev. B **93**, 214513 (2016).

[44] See Supplemental Material at http://link.aps.org/supplemental/10.1103/PhysRevB.95.075139 for further details of fitting and spin-wave theory.

[45] W. J. Padilla, M. Dumm, S. Komiya, Y. Ando, and D. N. Basov, Phys. Rev. B **72**, 205101 (2005).

[46] R. E. Cohen, W. E. Pickett, and H. Krakauer, Phys. Rev. Lett. **64**, 2575 (1990).

[47] C.-Z. Wang, R. Yu, and H. Krakauer, Phys. Rev. B **59**, 9278 (1999).

[48] M. Minola, G. Dellea, H. Gretarsson, Y. Y. Peng, Y. Lu, J. Porras, T. Loew, F. Yakhou, N. B. Brookes, Y. B. Huang, J. Pelliciari, T. Schmitt, G. Ghiringhelli, B. Keimer, L. Braicovich, and M. Le Tacon, Phys. Rev. Lett. **114**, 217003 (2015).

[49] C. J. Jia, E. A. Nowadnick, K. Wohlfeld, Y. F. Kung, C.-C. Chen, S. Johnston, T. Tohyama, B. Moritz, and T. P. Devereaux, Nat. Commun. **5**, 3314 (2014).

[50] L. Braicovich, M. Minola, G. Dellea, M. Le Tacon, M. Moretti Sala, C. Morawe, J.-C. Peffen, R. Supruangnet, F. Yakhou, G. Ghiringhelli, and N. B. Brookes, Rev. Sci. Instrum. **85**, 115104 (2014).

[51] A. Macridin, M. Jarrell, T. Maier, and D. J. Scalapino, Phys. Rev. Lett. **99**, 237001 (2007).

[52] M. Vojta, Adv. Phys. **58**, 699 (2009).

[53] G. Xu, G. D. Gu, M. Hucker, B. Fauque, T. G. Perring, L. P. Regnault, and J. M. Tranquada, Nat. Phys. **5**, 642 (2009).